Journal of Medicinal Chemistry

Article

A Gadolinium Complex of 1,4,7,10-Tetraazacyclododecane-1,4,7-trisacetic acid (DO3A)-Ethoxybenzyl (EOB) Conjugate as a New Macrocyclic Hepatobiliary MRI Contrast Agent

Ah Rum Baek, Hee-Kyung Kim, Subin Park, Gang Ho Lee, Hyo Jeung Kang, Jae Chang Jung, Joon-Suk Park, Hun-Kyu Ryeom, Tae-Jeong Kim, and Yongmin Chang

J. Med. Chem., **Just Accepted Manuscript** • Publication Date (Web): 22 May 2017

ACS Publications

Journal of Medicinal Chemistry is published by the American Chemical Society. 1155 Sixteenth Street N.W., Washington, DC 20036

A Gadolinium Complex of 1,4,7,10-Tetraazacyclododecane-1,4,7-trisacetic acid (DO3A)-Ethoxybenzyl (EOB) Conjugate as a New Macrocyclic Hepatobiliary MRI Contrast Agent

Ah Rum Baek,[1,] Hee-Kyung Kim,[2] Subin Park,[3] Gang Ho Lee,[4] Hyo Jeung Kang,[5] Jae-Chang Jung,[3] Joon-Suk Park,[6] Hun-Kyu Ryeom,[7] Tae-Jeong Kim,[8,] and Yongmin Chang,[1,2,7*]*

[1]Department of Medical & Biological Engineering, [2]Department of Molecular Medicine & BK21 Plus KNU Biomedical Convergence Program, [3]Department of Biology, [4]Department of Chemistry, [5]Department of Pharmacy, [7]Department of Radiology, and [8]Institute of Biomedical Engineering Research, Kyungpook National University, 80 Daehakro, Bukgu, Daegu 702-701, Korea [6]Laboratory Animal Center, Daegu-Gyeongbuk Medical Innovation Foundation 41061 Chumbok-ro 80, Dong-gu, Daegu, Korea

Keywords: Gadolinium, Contrast agent, MRI, Liver, Chelate

Abstract

We report the synthesis of a macrocyclic Gd chelate based on a 1,4,7,10-tetraazacyclododecane-1,4,7-trisacetic acid (DO3A) coordinationn cage bearing an ethoxybenzyl (EOB) moiety and discuss its use as a T_1 hepatobiliary magnetic resonance imaging (MRI) contrast agent. The new macrocyclic liver agent shows high chelation stability and high r_1 relaxivity compared with linear-type Gd chelates, which are the current clinically approved liver agents. Our macrocyclic, liver-specific Gd chelate was evaluated in vivo through biodistribution analysis and liver MRI, which demonstrated its high tumor detection sensitivity and suggested that the new Gd complex is a promising contrast agent for liver cancer imaging.

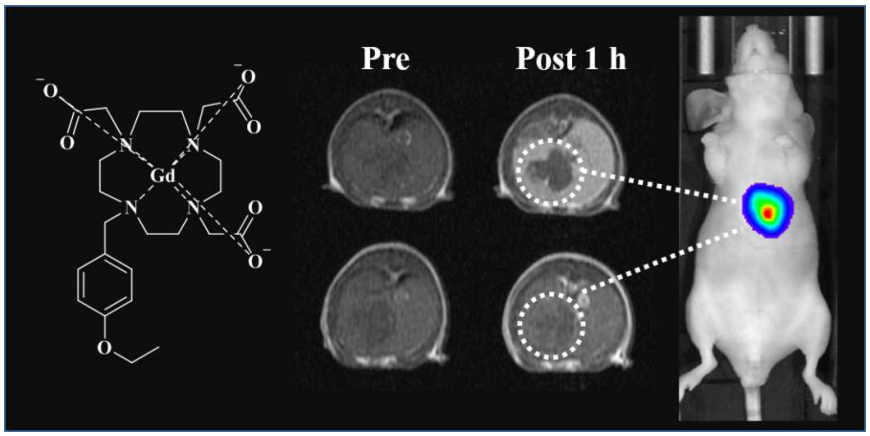

INTRODUCTION

Gd-based contrast agents (CAs) are the most commonly used clinical magnetic resonance imaging (MRI) CAs. By improving the visibility of specific organs, blood vessels, or lesions, these CAs help physicians diagnose and treat a wide variety of medical conditions.[1] Until 2006, it was believed that most, if not all, Gd was removed from the body rapidly after administration. However, in the last ten years, several studies have reported that elevated levels of Gd can remain in the body for a long period, which may cause nephrogenic systemic fibrosis (NSF) in patients with severe kidney disease.[2,3] NSF is a very serious clinical condition involving fibrosis of the skin and internal organs.[4-7] As exposure to Gd-based CAs has sharply increased owing to increased MRI examinations worldwide, concerns about the risk of NSF have also increased. More recently, researchers have found that, even in patients without severe renal dysfunction, the use of Gd-based CAs results in Gd accumulation in the brain.[8]

As safety concerns associated with the potential toxicity of Gd retained in the human body have increased, emphasis has been placed on the development of highly stable Gd complexes as CAs. In particular, the molecular structure of the Gd complex may contribute to the degree of Gd retention in the body; there are

two structurally distinct types of Gd complexes: linear and macrocyclic. Macrocyclic Gd complexes consist of a closed, cage-like ligand that surrounds and binds tightly to the Gd ion, forming highly stable complexes less likely to release free Gd into the body. Three macrocyclic Gd complexes are currently approved by the U.S. Food and Drug Administration (FDA): **8** (Gd-DOTA)[9], **9** (Gd-DO3A-butrol)[10], and **10** (Gd-HP-DO3A)[11]. Regarding biodistribution, as all these complexes are nonprotein binding, they are nonspecific extracellular agents.[12]

However, the design of highly stable liver-specific Gd complexes is challenging. Recently, two linear Gd complexes have been approved by the FDA as liver-specific MRI CAs: **11** (Gd-EOB-DTPA)[13] and **12** (Gd-BOPTA-DTPA)[14]. These liver-specific linear Gd complexes have similar stabilities to other nonspecific linear Gd complexes, including those associated with the greatest number of NSF cases.[15] There have been several attempts to synthesize liver-specific macrocyclic Gd complexes with high stability.[16-21] In this study, we designed and synthesized a new, highly stable macrocyclic Gd chelate based on a **7** (DO3A) coordination cage bearing ethoxybenzyl (EOB) moieties. First, we characterized the kinetic inertness of the complex with respect to transmetalation, relaxivity, hydration state, and the water exchange kinetics of

the macrocyclic Gd complex. In addition to forming a hydrophilic, stable complex with Gd ions, our detailed pharmacokinetic and biodistribution studies demonstrated that this new Gd chelate is rapidly taken up by hepatocytes. Therefore, this complex is a new, small Gd chelate based on a macrocyclic ligand that shows hepatobiliary specificity in vivo.

RESULTS AND DISCUSSION

Synthesis and Characterization

Scheme 1 shows the synthetic procedures for the ligand **5** and the corresponding Gd complex **6**. Compound **1** and **2** were prepared according to a literature method.[22] Chlorination of **2** with thionyl chloride in diethyl ether resulted in the formation of **3**, which was used without further purification. Ligand **5** was prepared by acid hydrolysis, with trifluoroacetic acid (TFA), of the corresponding *tert*-butyl ester ($_t$Bu), which in turn was prepared from the conjugate of $_t$*Bu* protected **7** with EOB moiety **3**. Complexation of Gd(III) by **5** led to the formation of the corresponding complex **6** as a hygroscopic white solid. Complex **6** was subsequently purified by preparative high-performance liquid chromatography (HPLC) (HPLC traces of **5** and **6** are shown in the Supporting Information, Figure S1 and S2). The formation of **5** and **6** was confirmed by microanalysis and spectroscopic techniques, such as ^{1}H NMR and

HR-FAB- or ESI-LC mass spectrometry (Figure 1 and Supporting Information, Figure S3).

Relaxivity

Table 1 shows the r_1 and r_2 relaxivities for **6**, along with those of **11** and **12**, which are supplied for comparative purposes. The most significant feature shown in Table 1 is that **6** exhibits higher r_1 values than any of the clinically used MRI CAs;[23] the r_1 value obtained for **6** is twice as high as that of **12**. The high relaxivity of **6** relative to those of the clinically used MRI CAs was expected considering that ligand **5** forms heptadentate complexes with Gd(III) ions.[24,25] Consequently, **6** can have two inner-sphere water molecules (q = 2), enabling more efficient relaxation.

Transmetalation Kinetics

In the human body, various endogenous metal ions are present, such as Zn(II), Cu(II), and Ca(II). These metal ions can compete with Gd(III) for the ligands, resulting in the loss of Gd ions,[26] which causes various diseases, such as NSF, or the deposition of Gd ions in the brain. In particular, the concentration of Zn(II) in human blood is higher (55–125 μM) than those of other metal ions, such as Cu(II) (1–10 μM). Moreover, the association constants toward DTPA

and DOTA are similar to those of Gd(III). Thus, it is important to assess the stability of Gd complexes in the presence of Zn(II) ions.

The kinetic inertness of **6** can be evaluated against those of clinically used MRI CAs in phosphate buffer (PBS). In the case of transmetalation by diamagnetic Zn(II) ions, insoluble $Gd_2(PO_4)_3$ is formed in PBS solution, and the paramagnetic relaxation rate of the solution decreases. Consequently, the normalized paramagnetic relaxation rate at a given time (R_1^p(t)/R_1^p(0)) can be used to measure the degree of transmetalation. Figure 2 shows that the cyclic octadentate **8** has high kinetic inertness, with more than 90% of the longitudinal relaxation rate maintained 72 h after the initial measurement. Complex **6**, which has a cyclic heptadentate structure, shows a relatively high kinetic stability compared with that of the octadentate group. The difference in the kinetic stability arises from differences in the coordination numbers of each complex. In contrast to acyclic complexes, the longitudinal relaxation rate maintained by **6** was considerably higher. Complex **6** maintained more than 75% of the initial longitudinal relaxation rate, whereas acyclic Gd complexes **11** and **12** maintained just 30–50% during the same measurement period.

Cell Viability Assay

Figure 3 shows the results of cell viability tests with **6**. The cells were incubated with the Gd complex for 24 h. The viability percentage of the cell line was almost 100% at all concentrations, indicating that **6** has negligible cell toxicity in the typical clinical concentration range. In addition, in normal hepatocyte cell toxicity tests, the proliferation percentage of **6** was similar to those of **8** and **11** over 72 h, as shown in the Supporting Information (Figure S4).

Biodistribution

The in vivo biodistribution of **6** was quantitatively measured by inductively coupled plasma atomic emission spectrometry (ICP-AES) (Figure 4). The clinical MR CAs, **8** and **11**, are used for comparative purpose. The ICP-AES data shows the high accumulation of **6** in the liver, at up to 50% of the administrated Gd dose. In case of **11**, it had faster liver accumulation rate than **6** within 30 min, reaching almost 50%. Whereas **8** presents typical ECF agent property without tissue-specific property. After 6 h, **6** was rapidly excreted from the liver. In addition to the liver, the kidneys and bladder show relatively high Gd accumulation, resulting from glomerular excretion via the renal pathway. Therefore, the in vivo biodistribution data strongly suggest that **6** is excreted by

both renal and hepatobiliary routes. This dual excretion pattern of **6** is very similar to the excretion pattern of the liver-specific linear Gd agent **11**.[27]

In Vivo MR Images of Normal Animals

In vivo MRI experiments were performed with **6** and liver-specific MRI CAs, such as **11** and **12**. Figure 5a–c shows the coronal T_1-weighted images, and Figure 5d–f shows the axial T_1-weighted images of 6-week-old male Institute of Cancer Research (ICR) mice treated with **6** and currently used liver MRI CAs.[28] The most characteristic features of **6** as a CA are that the signal enhancement in the liver and gallbladder is comparable with those of liver-specific CAs, such as **11** and **12**, and the contrast-to-noise-ratio (CNR) curves for **6**, **11**, and **12** show similar trends (Supporting Information, Figure S5). The CNR of **6** in the liver and gallbladder is slightly lower than those of **11** and **12**. However, this results from the higher initial renal excretion ratio of **6** at 20 min, as shown in Figure S5. All three liver-specific CAs show biliary excretion via the bile duct, confirming hepatobiliary uptake, as seen in Figure 5.[29,30] The clearance of **6** is confirmed by the T_1-weighted whole-body coronal images 24 h after intravascular injection (Supporting Information, Figure S6).

In Vivo MR Images of Liver Cancer Model

The induction of liver cancer in the mice was confirmed by bioluminescence imaging (Figure 6c). Using MRI, we made the liver cancer diagnosis using **6**. Figure 6a and b shows the axial T_1-weighted MR images of hepatocellular carcinoma (HCC) model nude mice; the images were obtained by tail vein injection with **6** (Figure 6a), as well as with **8** (Figure 6b), which was used for comparison. Unlike ECF agents, such as **8**, the new hepatobiliary MRI CA **6** is taken up by normal hepatocytes.[31,32] It is well-known that the human normal hepatocyte has hydrophobic drug-transporting proteins called organic anion-transporting polypeptides (OATPs) in its membrane, which play a significant role in drug absorption. Lipophilic xenobiotics can pass through the OATP drug transporters in normal liver tissue. However, OATPs are considerably decreased in most HCC.[33,34] Therefore, lipophilic organic drugs cannot pass through HCC cells, resulting in low MR intensity. These agents are thought to pass via OATP1 to the basolateral membrane of the hepatocyte. Thereafter, the agents are excreted via multidrug resistance protein 2 (MRP2).

The differences in uptake of **6** between normal hepatocytes and tumor cells demonstrate a significant difference in MR signal enhancement. Thus, the inflow of paramagnetic agents to the liver is greatly enhanced in normal

hepatocytes, as shown in Figure 6a. In contrast, liver cancer cells usually have abnormal OATP1 expression, resulting in inhibition of the uptake of **6** and the demonstration darker MR contrast compared with normal liver tissue. In the case of the nonspecific extracellular agent **8**, the MR images show indistinguishable contrast enhancement between normal liver tissue and tumor regions (Figure 6b). Therefore, **6** has significant clinical potential for detecting liver tumors and differentiating between normal liver cells and HCC.

CONCLUSION

The stability of Gd-based MRI CAs is of serious concern because free Gd (Gd^{3+}) is toxic and is associated with the development of NSF. Therefore, the ability of a ligand to bind tightly to Gd ions is an important safety consideration. In the current study, we designed and synthesized a new liver-specific macrocyclic Gd complex **6** for liver MRI, which has high chelation stability. Complex **6** showed much higher kinetic stability than liver-specific linear Gd complexes **11** and **12**. Furthermore, the r_1 relaxivity of **6** (8.07 mM^{-1} s^{-1}) was much higher than those of **11** and **12** (r_1 = 4.70 and 4.00 mM^{-1} s^{-1}, respectively). The biodistribution and in vivo MR images showed biliary excretion via the bile duct, confirming hepatobiliary uptake. To demonstrate the possible clinical potential for liver imaging, contrast-enhanced in vivo MR

images were obtained using **6** for the liver cancer animal model. MR images using **6** as a CA clearly demonstrated a significant difference in signal enhancement between normal liver and tumor tissues, whereas for the nonspecific extracellular agent **8**, no distinguishable contrast enhancement between the two tissue types was observed. Therefore, we conclude that, in every respect, macrocyclic complex **6** represents a new class of practical, liver-specific MRI CAs with significant benefits over its linear counterparts.

Experimental Methods

General Remarks

All commercial reagents were purchased from Aldrich or TCI and used as received unless otherwise stated. Deionized water was used for all experiments. The ^{1}H NMR experiments were carried out using a Bruker Advance 500 spectrometer at the Center for Instrumental Analysis, Kyungpook National University (KNU). NMR chemical shifts are given as δ values with reference to tetramethylsilane (TMS) as an internal standard and coupling constants are in Hz. High-resolution FAB-mass spectra were obtained using a JMS-700 model (Jeol, Japan) mass spectrophotometer at the Korean Basic Science Institute (KBSI). A HPLC system (LC-forte/R, Kyoto, Japan) equipped with a Luna 10 μm C18 column (250 × 21.2 mm, Pheonomenex, Inc., Torrance, CA, USA) and a UV-Vis detector (220 nm) was used for purifications and characterization. Elution conditions were as follows: (Method A) a mixture of an aqueous solution of TFA (0.1%, v/v) and an acetonitrile solution of TFA (0.1%, v/v), 10–100% acetonitrile solution over 25 min, flow rate = 12 mL/min. (Method B) an aqueous ammonium acetate solution (10 mM) and an acetonitrile solution of aq. ammonium acetate buffer (10 mM buffer, 10%, v/v), 20–100% acetonitrile solution over 35 min. Purities of **5** and **6** of >95% were obtained by preparative

reversed-phase HPLC with UV-vis detection at 220 nm (Supporting Information, Figure S1 and S2).

Synthesis and Characterization

4-Ethoxybenzaldehyde (1)

To a mixture of *p*-hydroxybenzaldehyde (4 g, 32.75 mmol) and K_2CO_3 (13.58 g, 98.26 mmol) in DMF (150 mL), ethyl bromide (2.69 mL, 36.03 mmol) was added dropwise. After stirring for 18 h at RT, K_2CO_3 residue was filtered and the filtrate was diluted with water (150 mL). Then, the solution was washed with diethyl ether (3 × 150 mL). The organic layers were dehydrated with anhydrous Na_2SO_4, and the solvent was evaporated under reduced pressure. Yield: 4.49 g (91.30%), ^{1}H NMR ($CDCl_3$); δ = 9.88 (*s*, 1H; CHO), 7.83 (*d*, *J* = 58.4 Hz, 2H; ArH), 6.99 (*d*, *J* = 58.4 Hz, 2H; ArH), 4.12 (*q*, *J* = 56.9 Hz, 2H; CH_2), 1.46 (*t*, *J* = 56.9 Hz, 3H; CH_3).

(4-Ethoxyphenyl)methanol (2)

$NaBH_4$ (0.83 g, 21.98 mmol) was gradually added to **1** (3 g, 19.98 mmol) in methanol (50 mL) at 0 °C. Then, the reaction mixture was stirred for 1 h at RT. When the reaction was completed, the solvent was evaporated under reduced pressure and water was added (80 mL). The mixture was extracted with ethyl

acetate (3 × 50 mL). The organic layer was dried over anhydrous $MgSO_4$, filtered, and evaporated to give a crude product, which was further purified by chromatography on silica (hexane/ethyl acetate, 7:3). Yield: 2.36 g (77.6%), ^{1}H NMR (DMSO-d_6); δ = 7.19 (*d*, 2H, *J* = 8.8 Hz), 6.82 (*d*, 2H, *J* = 8.4 Hz), 4.95 (*s*, 1H), 4.41 (*d*, 2H, *J* = 5.6 Hz), 3.96–4.02 (*m*, 2H), 1.32 (*t*, 3H, *J* = 7.2 Hz).

1-(Chloromethyl)-4-ethoxybenzene (3)

To compound **2** (3 g, 19.71 mmol) in diethyl ether (30 mL), thionyl chloride (2.86 mL, 39.42 mmol) was carefully added at 0 °C and stirred for 5 h at RT. The reaction mixture was extracted with saturated $NaHCO_3$ solution (3 × 30 mL). Subsequently, the diethyl ether layer was dried over anhydrous Na_2SO_4, filtered, and evaporated to obtain a pale yellowish oil. No further purification was carried out. Yield: 3.34 g (99.8%).

2, 2′, 2″-(10-(4-Ethoxybenzyl)-1,4,7,10-tetraazacyclododecane-1,4,7-triyl)triacetic acid (5)

To a mixture of *$_t$Bu* protected **7** (6.69 g, 20.28 mmol) and K_2CO_3 (5.60 g, 40.56 mmol) in acetonitrile (50 mL), a solution of **3** in acetonitrile (30 mL) was added dropwise at RT, and the mixture was stirred overnight. Any inorganic residues were removed by filtration, and then, acetonitrile was evaporated under

reduced pressure. The obtained crude product was dissolved in dichloromethane/TFA (1:1, 40 mL) at RT for deprotection of $_t$Bu. After 5 h, the solvent was removed under reduced pressure. The residue was precipitated in cold diethyl ether and then dried under vacuum. Further purification was accomplished using preparative HPLC, as follows: R_t = 10.45 min (Method A). The product was obtained by lyophilization as a hygroscopic white solid. Yield: 2.99 g (45.93%), HR-FABMS (*m/z*): calcd for $C_{23}H_{37}O_7N_4$: 481.2662 $[MH]^+$; found, 481.2662.

[Gd(DO3A-EOB)(H_2O)$_2$] (6)

Ligand **5** (0.36 g, 0.749 mmol) was dissolved in deionized water (10 mL), to which was added gadolinium(III) chloride hexahydrate (0.28 g, 0.749 mmol). The pH of reaction mixture was carefully adjusted to 7–7.5 with aq. NaOH (1 M). After 18 h, the solvent was evaporated to obtain the crude product, which was further purified by HPLC as follows: R_t = 15.92 min (Method B). Finally, the product was lyophilized to obtain a hygroscopic white solid. Yield: 0.24 g (50.20%), HR-FABMS (*m/z*): calcd for $C_{23}H_{33}GdN_4O_7Na$, 658.1494, $[MNa]^+$; found, 658.1494.

Relaxivity

T_1 measurements were carried out using an inversion recovery method with a variable inversion time (TI) at 1.5 T (64 MHz, GE Healthcare, Milwaukee, WI, USA). The MR images were acquired at 35 different TI values ranging from 50 to 1750 ms. T_1 relaxation times were obtained from the nonlinear least square fit of the signal intensity measured at each TI value. For T_2 measurements, the Carr–Purcell–Meiboom–Gill (CPMG) pulse sequence was adapted for multiple spin-echo (SE) measurements. The MR images were acquired at 34 different echo times (TEs) ranging from 10 to 1900 ms. T_2 relaxation times were obtained from the nonlinear least squares fit of the mean pixel values for multiple SE measurements at each TE. Subsequently, R_1 and R_2 relaxivities were calculated from the linear fit of each relaxation time with concentration (1, 0.5, 0.25, 0.125, and 0.0625 mM).

Transmetalation Kinetics

The kinetic inertness study was performed according to a literature method.[35,36] This method is based on measuring the evolution of the water proton longitudinal relaxation rate, $R_1^p(t)/R_1^p(0)$, of a buffer solution (PBS, pH 7.4) containing equimolar Gd complex and zinc chloride over time. The samples were prepared using a 2.5 mM solution of **6** solution of various

commercial MRI CAs, **8**, **11**, **12** and **13** (Gd-DTPA-BMA) as controls. Then, 10 μL of a 250 mM zinc chloride solution was added to 1 mL of a buffered solution of the Gd complex, and the mixture was vigorously stirred. The R_1^p relaxation rate was obtained after subtraction of the diamagnetic contribution of the water proton relaxation from the observed relaxation rate R_1. The measurements were carried out using a 3 T whole-body system (Magnetom Tim Trio, Simens, Korea Institute of Radiological & Medical Science) at RT.

Cell Viability Assay

In this study, human embryonic kidney cells (HEK-293), which are widely used for in vitro cell cytotoxicity evaluation, were chosen. Cells were maintained in Dulbecco's modified Eagle's medium (DMEM, Gibco) supplemented with heat-inactivated fetal bovine serum (FBS) (10%), penicillin (100 IU/mL), and streptomycin (100 mg/mL), which were all purchased from Gibco. The medium was replaced every 2 days, and the cells were split into a 96-well plate (1×10^4 cells/well/200 μL). Aqueous solutions of **6** (50–500 μM) were added into the serum-free media and incubated for 24 h. Then, cell counting kit-8 (CCK-8) (10 μL) was added to each well. The solution was removed after 4 h at 37 °C. The optical density at 450 nm was determined using a microplate reader (Bio-rad550 Reader, Molecular Devices, Sunnyvale, CA,

USA) to evaluate the cell cytotoxicity.[37] In addition, normal hepatocytes were used to test Gd toxicity in the liver environment over 72 h. The methodology for the normal cell proliferation test was the same as that used for the above HEK-293 cell viability test.

Biodistribution

Complex **6** was administrated intravenously as a bolus in a tail vein of a 6-week-old male mouse (ICR, 25–27 g). The mice were anesthetized and killed by means of exsanguinations from the vena cava at each time point (0.5, 1, 6, and 24 h after injection time). The Gd concentration was measured in tissues (liver, spleen, intestine, heart, lung, kidneys, bladder, bile duct, and blood). In addition, the Gd concentration was determined by digesting the tissues with nitric acid (70%) at 180 °C for 120 min and measuring the concentration in the clear diluted solution by ICP-AES (Optima, 7300DV, PerkinElmer, Waltham, MA, USA). The detection limit of this method is 0.01 ppm.[38]

Orthotopic Xenograft Mouse Model

The orthotopic xenograft mouse model was approved by the Institutional Animal Care and Use of Committee of Daegu-Gyeongbuk Medical Innovation Foundation (DGMIF) and performed in accordance with protocols approved by

the Institutional Animal Care and Use of Committee. Five-week-old male athymic nude (BALB/c nu/nu) mice were purchased from Orient Bio (Seongnam, Korea) and housed in a specific pathogen-free facility at the Laboratory Animal Center of DGMIF before use. The mice were inoculated with luciferase-expressing human liver cancer cells (HepG2-luc2) (1×10^6 cells in 50 μL HBSS), which were purchased from Perkin Elmer Inc. and were grown in Eagle's minimum essential medium (EMEM) (American Type Culture Collection [ATCC]) containing 10% FBS) in the subcapsular parenchymal of the left liver lobe. Four weeks after inoculation, the mice were imaged using an in vivo imaging system (IVIS).

Bioluminescence Imaging

Mice were intraperitoneally administered firefly D-luciferin potassium salt at a dose of 150 mg/kg body weight in Dulbecco's PBS. Bioluminescence images were acquired with the IVIS Lumina system (PerkinElmer). Image analysis was performed using Living Image software by measuring the photon flux (photons/[s·cm^2·steradian]). The signal intensity was measured for approximately 1 h, until it decayed considerably. Serial images were obtained from all animals, and the mean photon flux relative to the peak signal was determined.

In Vivo MRI Experiments

The in vivo MRI experiments were performed in accordance with the rules of the animal research committee of Kyungpook National University (KNU). In these studies, six-week male ICR mice with weights of 25–27 g were used. The mice were anesthetized by 1.5% isoflurane in oxygen. MR images were acquired before and after tail vein injection of each MRI CA (**6**, **11** and **12**). The CA injection dose was 0.1 mmol Gd/kg for MR images. After each measurement, the mice were revived from anesthesia and placed in the cage with free access to food and water. During these measurements, the animals were maintained at approximately 37 °C using a warm water blanket.

MR images were acquired with a 1.5 T system (GE Healthcare, Milwaukee, WI, USA) equipped with a homemade birdcage-shaped RF coil for small animals. The coil was of the receiver type with an inner diameter of 50 mm. The image parameters of the coronal images for SE measurements were as follows: repetition time (TR) = 300 ms; echo time (TE) = 13 ms; field of view (FOV) = 11 mm; 192 × 128 matrix size; 1.2 mm slice thickness; number of acquisition (NEX) = 8; and scan time of each image = 2 min 37 s. Those of the axial images were as follows: TR = 300 ms; TE = 13 ms; FOV = 6 mm; 192 × 128 matrix size; 1.5 mm slice thickness; NEX = 4; spacing = 0.4; and scan time of each image: 2 min 41 s. MR images were obtained 24 h after injection.

The anatomical locations with enhanced contrast were identified for liver, bile duct, heart, and kidney in post-contrast MR images. For quantitative measurements, the signal intensities in specific regions of interest (ROI) were measured using Advantage Window software (GE Medical, USA). The CNR was calculated using eq. (1), where SNR is the signal-to-noise ratio.[39]

$$\mathrm{CNR} = \mathrm{SNR}_{post} - \mathrm{SNR}_{pre} \quad (1)$$

Liver Cancer In Vivo MR Images

In this in vivo MR study, **6** and **8** were tail-vein injected into liver cancer model mice at a dosage of 0.1 mmol Gd/kg. As a liver cancer cell line, HepG2 cells were introduced into the livers of 5-week-old male nude mice (20–21 g). The MR images were collected using a 1.5 T system equipped with a homemade birdcage-type coil for small animals. A fast SE sequence was used to verify the liver cancer region using a T_2-weighted image and the following image parameters: TR = 2000 ms; TE = 40 ms; FOV = 8 mm; 256 × 192 matrix size; 2.0 mm slice thickness; NEX = 8; scan time of each image = 2 min 44 s; and flip angle (FA) = 10°. In sequence, the T_1-weighted image was obtained to estimate the liver cancer diagnosis capability of **6**. The parameters for the T_1-weighted coronal images are as follows (those for the axial images are given in

parentheses): TR = 300 ms; TE = 13 ms; FOV = 11 mm (6 mm); 192 × 128 matrix size; 1.2 mm slice thickness (1.5 mm); NEX = 8.00 (4.00); scan time = 2 min 37 s (2 min 41 s).

ASSOCIATED CONTENT

Supporting Information

The Supporting Information is available free of charge on the ACS Publications website at DOI:

Molecular formula strings (CSV)

CNR profiles and coronal T_1-weighted whole body MR images

Chemical compound characterization (High-resolution FAB mass, HPLC spectra)

Cell proliferation data

AUTHOR INFORMATION

Corresponding Authors

* For Y.C.: Phone, (+)82-53-420-5471; E-mail, ychang@knu.ac.kr

* For T.J.K.: Phone, (+)82-53-950-4127; E-mail, tjkim@knu.ac.kr

Authors to whom correspondence should be addressed

Author Contributions

The manuscript was written through contributions of all authors. All authors have given approval to the final version of the manuscript.

ACKNOWLEDGMENTS

This work was supported by the Basic Research Laboratory (BRL) Program (2013R1A4A1069507) and by the Basic Science Research Program (Grant No. 2017R1A2B3003214) through the National Research Foundation funded by the Ministry of Science, ICT and Future Planning.

ABBREVIATIONS

DO3A, 1, 4, 7, 10-tetraazacyclododecane-1, 4, 7-trisacetic acid; DTPA, diethylenetriaminepentaacetic acid; DOTA, tetraazacyclododecane-1, 4, 7, 10-tetraacetic acid; EOB, Ethoxybenzyl; BOPTA, benzyloxypropionoic-tetraacetate; Gd-DOTA, gadoterate meglumine; Gd-HP-DO3A, gadoteridol;

Gd-DO3A-butrol, gadobutrol; Gd-EOB-DTPA, gadoxetic acid; Gd-BOPTA-DTPA, gadobenate dimeglumine; HPLC, high performance liquid chromatography; MRI, magnetic resonance imaging; NSF, nephrogenic systemic fibrosis; GB, gallbladder; OATP, organic anion transporter polypeptide; MRP, multidrug resistance protein; ECF, extracellular fluid; TI, inversion time; CPMG, Carr−Purcell−Meiboon−Gill pulse sequence; TE, echo time; TR, repetition time; SE, spin echo; FOV, field of view; NEX, number of acquisition; ROI, regions of interest; CNR, contrast to noise ratio; CAs, contrast agents; HCC, hepatocellular carcinoma; CCK-8, cell counting kit-8; PBS, phosphate buffered saline; DMEM, Dulbecco's modified eagle's medium; ICP, inductively coupled plasma; EMEM, eagle's minimum essential medium; FBS, fetal bovine serum; IVIS, in vivo imaging system; HepG2-luc2, luciferase expressing human liver cancer cell line.

REFERENCES

(1) Maureen. M.; Linda. B.; Release gadolinium may remain in brain after contrast MRI. *RSNA. Press Release.* [Online] **2015**, https://press.rsna.org/timssnet/media/pressreleases/14_pr_target.cfm?ID=810. Accessed September 10, 2016.

(2) Penfield, J. G.; Reilly, R. F. What nephrologists need to know about gadolinium. *Nat. Clin. Pract. Nephrol.* **2007**, *3*, 654–668.

(3) Perez-Rodriguez, J.; Lai, S.; Ehst, B. D.; Fine, D. M.;Bluemke, D. A. Nephrogenic systemic fibrosis: incidence, associations, and effect of risk factor assessment—report of 33 Cases. *Radiology* **2009***, 250*, 371-377.

(4) Abu-Alfa, A.K. Nephrogenic systemic fibrosis and gadolinium-based contrast agents. *Adv. Chronic Kidney Dis*. **2011**, *18*, 188-198.

(5) Idée, J.M.; Fretellier, N.; Robic, C.; Corot, C. The role of gadolinium chelates in the mechanism of nephrogenic systemic fibrosis: a critical update. *Crit. Rev. Toxicol*. **2014**, *44*, 895-913.

(6) Amie, S.; Caravan, P. Biodistribution of gadolinium-based contrast agents, including gadolinium deposition. *J. Magn. Res. Imag.* **2009**, *30*, 1259-1267.

(7) Sieber, M. A.; Lengsfield, P.; Frenzel, T.; Golfier, S.; Schmitt-Willich, H.; Siegmund, F.; Walter, J.; Weinmann, H-J.; Pietsch, H. Preclinical investigation to compare different gadolinium-based contrast agents regarding their propensity to release gadolinium in vivo and to trigger nephrogenic systemic fibrosis-like lesions. *Eur. Radiol.* **2008**, *18*, 2164-2173.

(8) Kanal, E.; Tweedle, M. F. Residual or retained gadolinium: practical implications for radiologists and our patients. *Radiology* **2015**, *275*, 630-634.

(9) Meyer, D.; Schaefer, M.; Bonnemain, B. Gd-DOTA, a potential MRI contrast agents: current status of physicochemical knowledge. *Invest. Radiol.* **1988**, *23,* S232-S235.

(10) Vogler, H.; Platzek, J.; Schuhmann-Giampieri, G.; Frenzel, T.; Weinmann, H-J.; Raduchel, B.; Press, W-R. Pre-clinical evaluation of gadobutrol: a new, neutral, extracellular contrast agent for magnetic resonance imaging. *Eur. J. Radiology* **1995**, *21*, 1-10.

(11) Glogard, C.; Hovland, R.; Fossheim, S. L.; Aasen, A. J.; Klaveness, J. Synthesis and physicochemical characterisation of new amphiphilic gadolinim DO3A complexes as contrast agents for MRI. *J. Chem. Soc. Perkin Trans 2* **2000**, *2*, 1047-1052.

(12) Michael, F. T.; Emanuel K.; Robert M. Considerations in the selection of a new gadolinium-based contrast agent. *Appl. Radiol.* **2014**, *1*, 1-11

(13) Hamm, B.; Staks, T.; Mühler, A.; Bollow, M.; Taupitz, M.; Frezel, Z.; Wolf, K. J.; weinmann, H. J.; Lange, L. Phase 1 clinical evaluaion of Gd-EOB-DTPA as a hepatobiliary MR contrast agent: safrty, phamacokinetics, and MR imaging. *Radiology* **1995**, *195*, 785-792.

(14) Vittadini, G.; Felder, E.; Musu, C.; Tirone, P. Preclinical profile of Gd-BOPTA a liver-specific MRI contrast agent. *Invest. Radiol.* **1990**, *25*, S59-S60.

(15) Ramalho, X. J.; Semelka, X. R. C.; Ramalho, X. M.; Nunes, X. R. H.; Alobaidy, X. M.; Castillo, X. M. Gadolinium-based contrast agent accumulation and toxicity: an update. *Am. J. Neuroradiol.* **2016***, 37*, 1192-1198.

(16) Harrison, A.; Walker, C.A.; Pereira, K.A.; Parker, D.; Royle, L.; Pulukkody, K.; Norman, T.J. Hepato-biliary and renal excretion in mice of charged and neutral gadolinium complexes of cyclic tetra-aza-phosphinic and carboxylic acids. *Magn. Reson. Imaging* **1993**, *11*, 761-770.

(17) Runge, V.M.; Wells, J.W.; Williams, N.M. Comparison of gadolinium Cy2DOTA, a new hepatobiliary agent, and gadolinium HP-DO3A, an extracellular agent, in healthy liver and metastatic disease. *Invest. Radiol.* **1995**, *30*, 123-130.

(18) Runge, V. M.; Wells, J.W.; Williams, N.M. Evaluation of gadolinium 2,5-BPA-DO3A, a new macrocyclic hepatobiliary chelate, in normal liver and metastatic disease on high field magnetic resonance imaging. *Invest. Radiol.* **1996**, *31*, 11-16.

(19) Marinelli, E.R.; Neubeck, R.; Song, B.; Wagler, T.; Ranganathan, R.S.; Sukumaran, K.; Wedeking, P.W.; Nunn, A.; Runge, V.M.; Tweedle, M.F. Synthesis, characterization, and imaging performance of a new class of macrocyclic hepatobiliary MR contrast agents. *Invest. Radiol.* **2000**, *35*, 8-24.

(20) Chong, H. S.; Garmestani, K.; Henry Briant, L.; Milenic, D. E.; Overstreet, T.; Birch, N.; Le, T.; Brady, E. K.; Brechbiel, M. W. Synthesis and evaluation of novel macrocyclic and acyclic ligands as contrast enhancement agents for magnetic resonance imaging. *J. Med. Chem.* **2006**, *46*, 2055-2062.

(21) Muhler, A.; Platzek, J.; Raduchel, B.; Frenzel, T.; Weinmann, H-J. Characterization of a gadolinium-labeled cholesterol derivative as an organ-soecific contrast agent for adrenal MR imaging. *J. Magn. Res. Imag.* **1995**, *5*, 7-10.

(22) Eleftheriadis, N.; Thee, S.; te Biesebeek, J.; van der Wouden, P.; Baas, B. J.; Dekker, F. J. dentification of 6-benzyloxysalicylates as a novel class of inhibitors of 15-lipoxygenase-1. *Eur. J. Med. Chem.* **2015**, *94*, 265–275.

(23) Rohrer, M.; Bauer, H.; Mintorovitch, J.; Requardt, M.; Weinmann, H.-J. Comparison of magnetic properties of MRI contrast media solutions at different magnetic field strengths. *Invest. Radiol.* **2005**, *40*, 715–724.

(24) Zhang, X.; Chang, C. A.; Brittain, H. G.; Garrison, J. M.; Telser, J.; Tweedle, M. F. pH dependence of relaxivities and hydration numbers of gadolinium(III) complexes of macrocyclic amino carboxylates. *Inorg. Chem.* **1992***, 31*, 5597–5600.

(25) Chang, C. A.; Brittain, H. G.; Telser, J.; Tweedle, M. F. ID 170 pH Dependence of relaxivities and hydration numbers of gadolinium complexes of linear amino carboxylates. *Inorg. Chem.* **1990**, *29*, 4468–4473.

(26) McDonald, R. J.; McDonald, J. S.; Kallmes, D. F.; Jentoft, M. E.; Murray, D. L.; Thielen, K. R.; Williamson, E. E.; Eckel, L. J. Intracranial gadolinium deposition after contrast-enhanced MR imaging. *Radiology* **2015***, 275*, 772-782.

(27) Weinmann, H. J.; Schuhmann-Giampieri, G.; Schmitt-Willich, H.; Vogler, H.; Frenzel, T.; Gries, H. A new lipophilic gadolinium chelate as a tissue-specific contrast medium for MRI. *Magn. Reson. Med.* **1991**, *22*, 233–237; discussion 242.

(28) Gu, S.; Kim H.-K.; Lee, G.-H.; Kang, B.-S.; Chang, Y.; Kim, T.-J. Gd-complexes of 1,4,7,10-tetraazacyclododecane-N,N’,N’’,N’’’-1,4,7,10-tetraacetic

acid (DOTA) conjugates of tranexamates as a new class of blood-pool magnetic resonance imaging contrast agents. *J. Med. Chem.* **2011**, *54*, 143–152.

(29) Müller, M.; Jansen, P. L. Molecular aspects of hepatobiliary transport. *Am. J. Physiol.* **1997**, *272*, G1285–G1303.

(30) Leonhardt, M.; Keiser, M.; Oswald, S.; Kühn, J.; Jia, J.; Grube, M.; Kroemer, H. K.; Siegmund, W.; Weitschies, W. Hepatic uptake of the magnetic resonance imaging contrast agent Gd-EOB-DTPA: role of human organic anion transporters. *Drug. Metab. Dispos.* **2010**, *38*, 1024–1028.

(31) Seale, M. K.; Catalano, O. A.; Saini, S.; Hahn, P. F.; Sahani, D. V. Hepatobiliary-specific MR contrast agents: role in imaging the liver and biliary tree. *Radiographics* **2009**, *29*, 1725–1748.

(32) Kiryu, S.; Inoue, Y.; Watanabe, M.; Izawa, K.; Shimada, M.; Tojo, A.; Yoshikawa, K.; Ohtomo, K. Evaluation of gadoxetate disodium as a contrast agent for mouse liver imaging: comparison with gadobenate dimeglumine. *Magn. Reson. Imaging* **2009**, *27*, 101–107.

(33) Van Beers, B. E.; Pastor, C. M.; Hussain, H. K. Primovist, eovist: What to expect? *J. Hepatol.* **2012**, *57*, 421–429.

(34) Vilgrain, V.; Van Beers, B. E.; Pastor, C. M. Insights into the diagnosis of hepatocellular carcinomas with hepatobiliary MRI. *J. Hepatol.* **2016**, *64*, 708–716.

(35) Laurent, S.; Elst, L. V.; Copoix, F.; Muller, R. N. Stability of MRI maramagnetic contrast media: a proton relaxometric protocol for transmetallation assessment. *Invest. Radiol.* **2001**, *36*, 115–122.

(36) Polasek, M.; Caravan, P. Is macrocycle a synonym for kinetic inertness in Gd(III) complexes? Effect of coordinating and noncoordinating substituents on inertness and relaxivity of Gd(III) chelates with DO3A-like ligands. *Inorg. Chem.* **2013**, *52*, 4084–4096.

(37) Kim, H.-K.; Kang, M.-K.; Jung, K.-H.; Kang, S.-H.; Kim, Y.-H.; Jung, J. C.; Lee, G. H.; Chang, Y.; Kim, T.-J. Gadolinium complex of DO3A-benzothiazole aniline (BTA) conjugate as a theranostic agent. *J. Med. Chem.* **2013**, *56*, 8104–8111.

(38) Jung, K.-H.; Kim, H.-K.; Park, J.-A.; Nam, K.-S.; Lee, G. H.; Chang, Y.; Kim, T.-J. Gd complexes of DO3A-(biphenyl-2,2′-bisamides) conjugates as MRI blood-pool contrast agents. *ACS Med. Chem. Lett.* **2012**, *3*, 1003–1007.

(39) Nam, K.-S.; Jeong, H.-J.; Kim, H.-K.; Choi, G.; Suh, K.-J. Gadolinium complex of 1 , 4 , 7 , 10-tetraazacyclododecane- N , N' , N'' , N''' -1 , 4 , 7-

trisacetic Acid (DO3A) conjugate of tranexamates : a quest for a liver-specific magnetic resonance imaging contrast agent . *Bull. Korean Chem. Soc.* **2014**, *35*, 1–4.

Table 1. r_1 and r_2 values for **6** and clinical used liver-specific MRI CAs in water at 25 °C (298.15 K)

	r_1 (mM^{-1}s^{-1})	r_2 (mM^{-1}s^{-1})
6	8.07 ± 0.09	8.54 ± 0.15
11	4.70 ± 0.40[a]	5.10 ± 1.2[a]
12	4.00 ± 0.40[a]	4.30 ± 1.0[a]

Scheme 1. Synthesis procedure of **6**

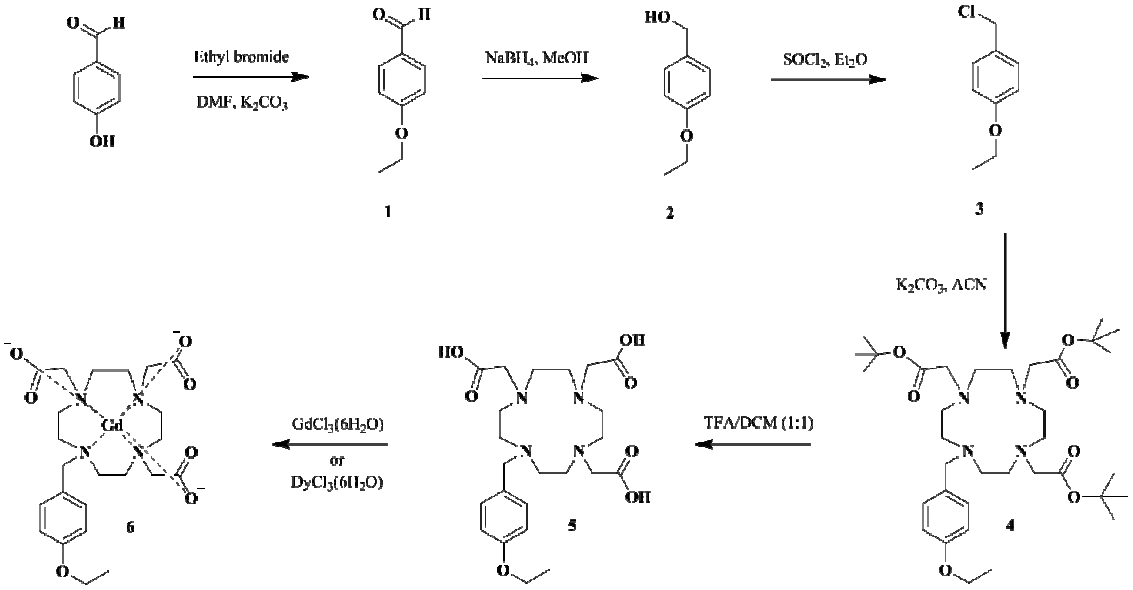

Scheme 2. Clinical MRI CAs and cyclic ligand

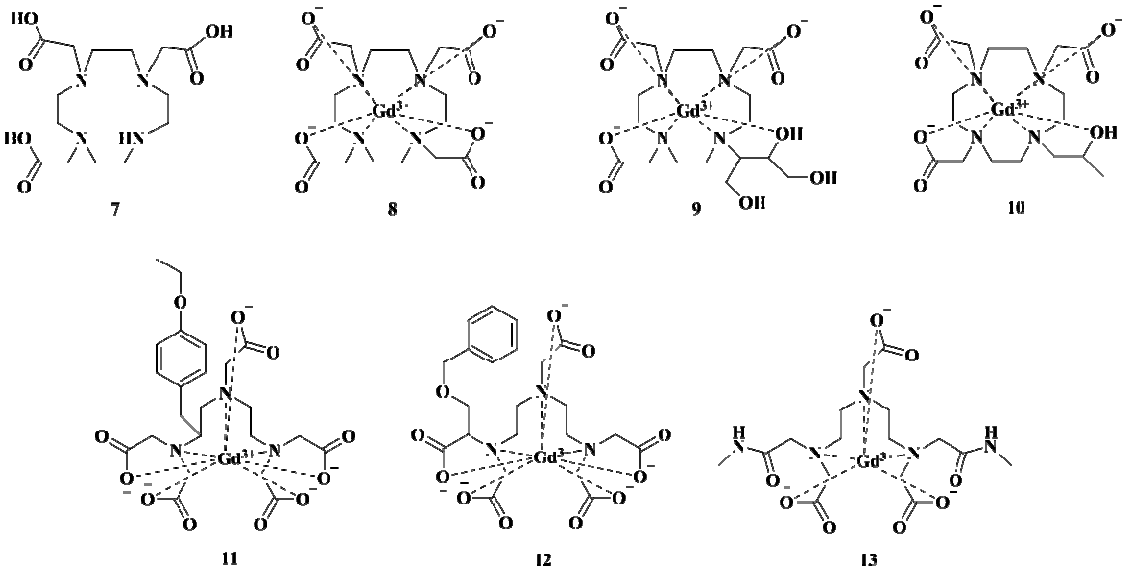

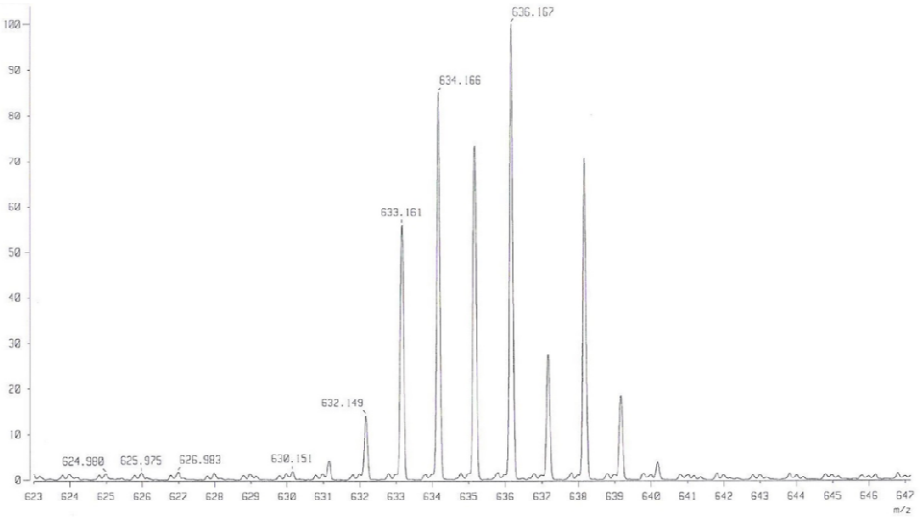

Figure 1. High-resolution FABMS of **6**

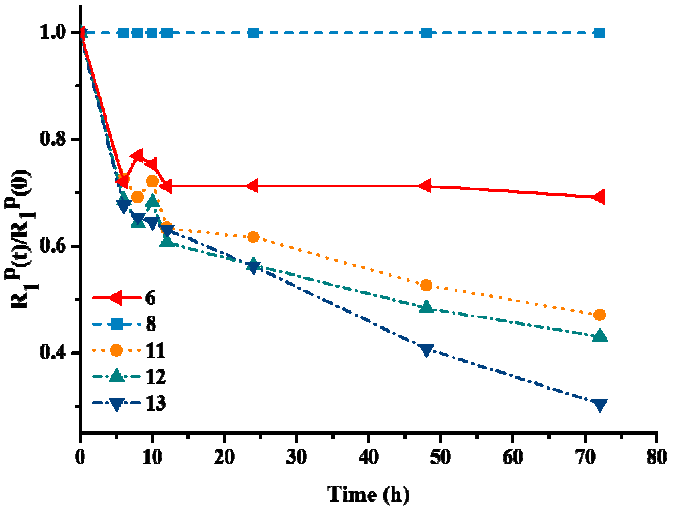

Figure 2. Evolution of paramagnetic relaxation rate, $R_1^P(t)/R_1^P(0)$, as a function of time for **6** and clinical used MRI CAs

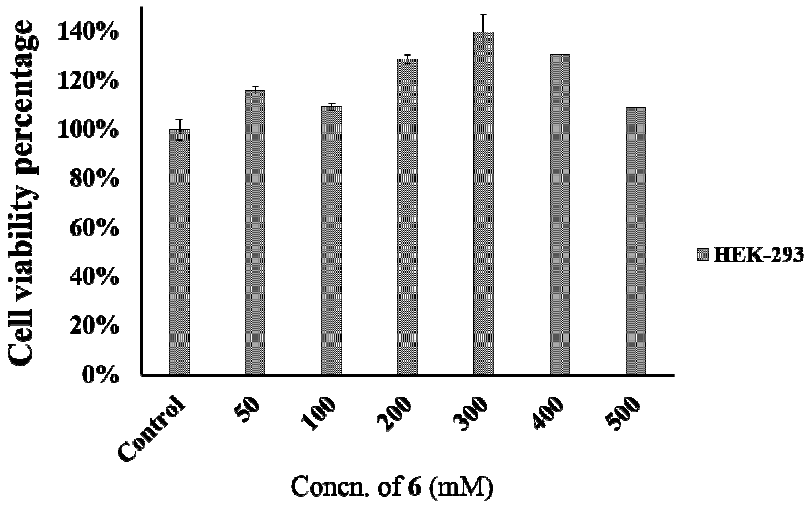

Figure 3. Relative cell viability (%) the human embryonic kidney cells (HEK-293) obtained by **6**

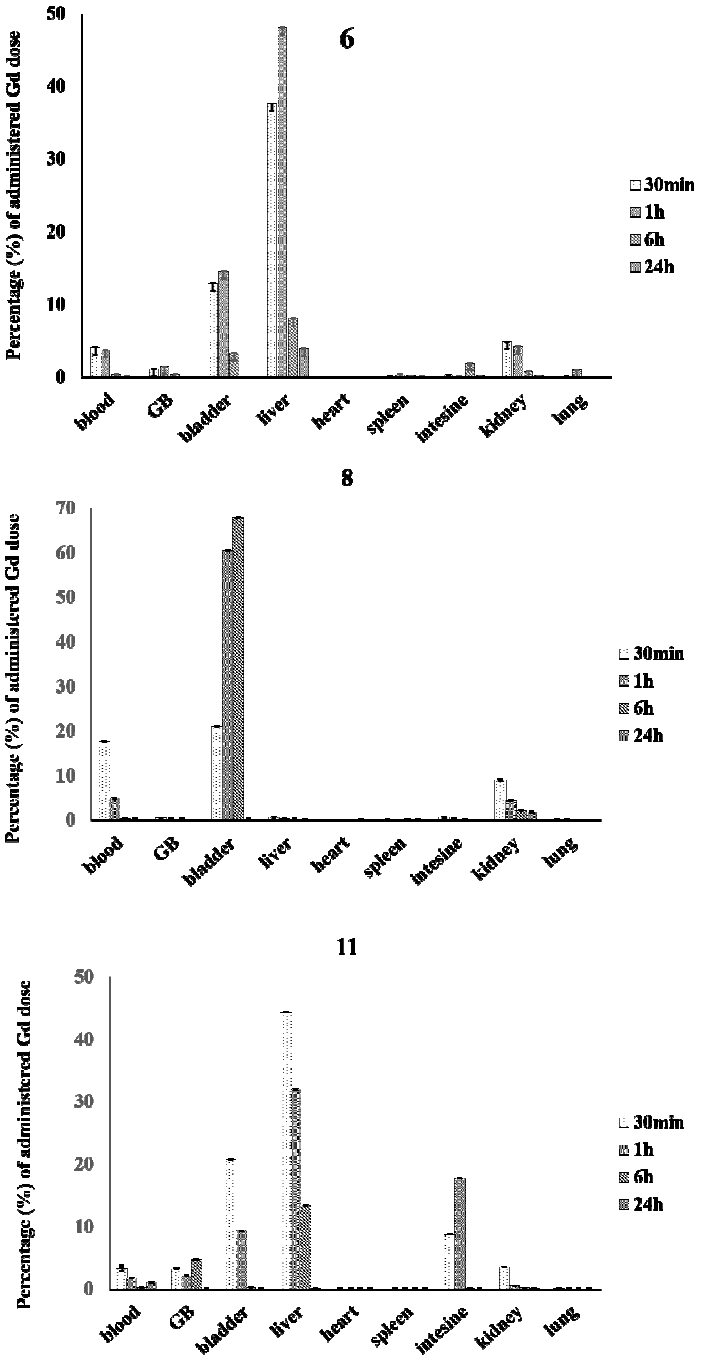

Figure 4. Time-dependent biodistribution data of **6**, **8** and **11** in normal ICR mice (n=4) with 0.1 mmol Gd/kg dosage.

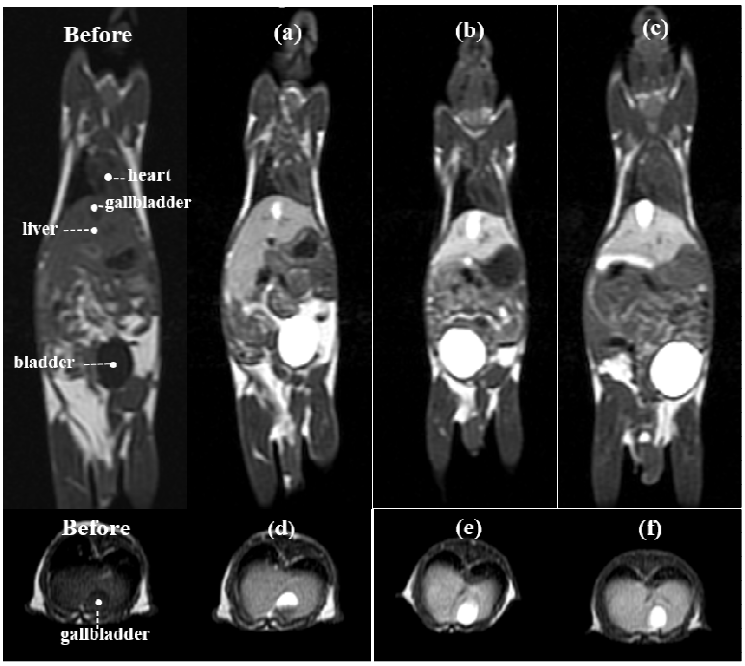

Figure 5. T_1-weighted whole body MR images of six-week male ICR mice; pre and post-injection images after 1h with 0.1 mmol Gd/kg dosage; (a) **6**; (b) **11** and (c) **12** for coronal images. And (d) **6**; (e) **11**; (f) **12** for abdominal axial images.

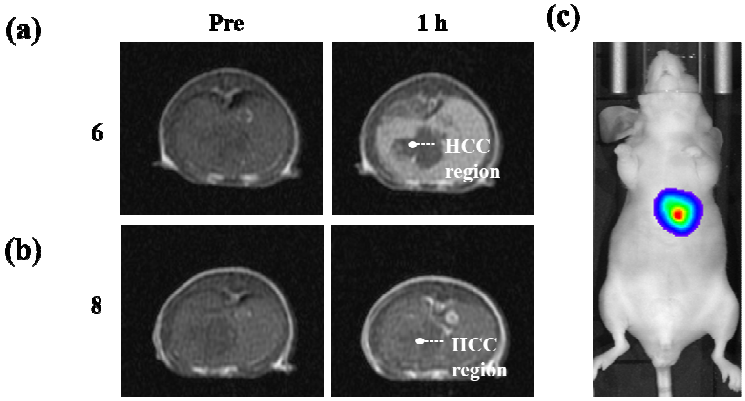

Figure 6. Axial T_1-weighted MR image of HCC model nude mice Each MR CAs administered intravascularly at 0.1 mmol Gd/kg. The image groups are composed with pre- and post-injected images (1h after injection). HCC regions are marked with white arrow. (a) **6**; (b) **8**. And (c) bioluminescence image of orthotopic xenograft mouse model for confirming HCC lesion.

Table of Contents graphic